2019

M^2 Factor of a Vector Schell-Model Beam

Milo W. Hyde IV
Air Force Institute of Technology

Mark F. Spencer

Optical Engineering

OpticalEngineering.SPIEDigitalLibrary.org

M^2 factor of a vector Schell-model beam

Milo W. Hyde, IV
Mark F. Spencer

SPIE.

Milo W. Hyde, IV, Mark F. Spencer, "M^2 factor of a vector Schell-model beam," *Opt. Eng.* **58**(7), 074101 (2019), doi: 10.1117/1.OE.58.7.074101.

M^2 factor of a vector Schell-model beam

Milo W. Hyde IV[a,*] **and Mark F. Spencer**[b]
[a]Air Force Institute of Technology, Department of Electrical and Computer Engineering, Dayton, Ohio, United States
[b]Air Force Research Laboratory, Directed Energy Directorate, Kirtland Air Force Base, New Mexico, United States

Abstract. Extending existing scalar Schell-model source work, we derive the M^2 factor for a general electromagnetic or vector Schell-model source to assess beam quality. In particular, we compute the M^2 factors for two vector Schell-model sources found in the literature. We then describe how to synthesize vector Schell-model beams in terms of specified, desired M^2 and present Monte Carlo simulation results to validate our analysis.
 [DOI: 10.1117/1.OE.58.7.074101]

Keywords: beam quality; coherence; optical simulations; Schell-model; statistical optics; vector sources.

Paper 190565 received Apr. 25, 2019; accepted for publication Jun. 7, 2019; published online Jul. 10, 2019.

In the early 1990s, Siegman proposed the M^2 factor as a metric to assess laser beam quality.[1] Siegman defined the M^2 factor as the ratio of a test beam's space-beamwidth product to that of an ideal Gaussian TEM_{00} beam. In so doing, he showed that the test beam's spot size $W_x(z)$ (in the x direction as a function of range z) obeyed the quadratic propagation formula:

$$W_x^2(z) = W_x^2(z_0) + M_x^4 \frac{\lambda^2}{\pi^2 W_x^2(z_0)}(z - z_0)^2, \tag{1}$$

where λ is the wavelength, z_0 is the z location of the waist plane, and $W_x(z_0)$ is the test beam's spot size in the waist plane, i.e., $W_x(z_0)$ is the test beam's waist. Expressed in this form, the physical interpretation of M^2 becomes clear: $M^2 \geq 1$ is the test beam's far-zone (FZ) beam spread relative to an ideal Gaussian beam with a waist equal to that of the test beam.

Siegman's M^2 quickly gained acceptance and became the laser industry's standard for assessing beam quality. It was soon extended to include hard-aperture,[2,3] vortex,[4] and stochastic, or partially coherent beams.[5–8] The latter, which are germane to this work, focus exclusively on scalar partially coherent beams. There have been several papers that derived the M^2 factors for specific electromagnetic (EM) or vector partially coherent beams, e.g., EM Gaussian Schell-model (EGSM) beams.[9–12] However, none to date have derived an expression for the M^2 factor of a general EM Schell-model beam.

This analysis is useful considering the wide-spread use of M^2 to assess beam quality and a large number of vector Schell-model sources that have been developed for applications, such as free-space/underwater optical communications, directed energy, optical trapping/tweezers, etc.[13–26] For directed energy, in particular, the use of M^2 to describe beam quality is pervasive, and there has been recent work in modeling dynamic, stochastic, noncommon-path phase errors in high-energy-laser systems in terms of M^2.[27] Most importantly, having a relation for the M^2 factor of a general EM Schell-model source allows one to consider beam quality in the design of new vector Schell-model beams.

For the reasons stated above, here, we extend the scalar partially coherent source M^2 analysis presented in Refs. 5 and 6 to vector Schell-model beams. Starting with Siegman's M^2 definition, we derive an expression for the M^2 factor of a vector partially coherent source in terms of the vector component beam quality factors. We then apply the results in Refs. 5 and 6 to derive a simple and physical relation for the M^2 factor of a general vector Schell-model beam. We present examples, where we calculate M^2 for two EM Schell-model sources using our M^2 relation and describe how to synthesize vector Schell-model beams in terms of specified, desired M^2.

In Sec. 2, we present Monte Carlo simulations, where we generate two examples of EM Schell-model sources in terms of M^2 to validate our analysis. We then study the convergence of the stochastic vector field realizations to the specified, desired M^2. Last, we conclude this paper with a summary of the work presented herein.

1 Theory

In this section, we first review the scalar M^2 theory found in Refs. 5 and 6. Next, we calculate the M^2 factors for two example vector Schell-model sources. We then describe how to generate vector Schell-model beams in terms of specified, desired M^2.

1.1 *Siegman's M²*

As defined by Siegman,[1] the M^2 factor in the x direction M_x^2 is as follows:

$$M_x^2 = 4\pi\sigma_x\sigma_{f_x}, \tag{2}$$

with a similar definition for M_y^2. The normalized beam widths σ_x and σ_{f_x} are as follows:

*Address all correspondence to Milo W. Hyde IV, E-mail: milo.hyde@us.af.mil

$$\sigma_x^2 = \frac{\iint_{-\infty}^{\infty}(x-\langle x\rangle)^2 \mathrm{Tr}[\underline{\mathbf{W}}(\boldsymbol{\rho},\boldsymbol{\rho})]\mathrm{d}^2\rho}{\iint_{-\infty}^{\infty}\mathrm{Tr}[\underline{\mathbf{W}}(\boldsymbol{\rho},\boldsymbol{\rho})]\mathrm{d}^2\rho}$$
$$= \frac{\iint_{-\infty}^{\infty}(x-\langle x\rangle)^2 S_x(\boldsymbol{\rho})\mathrm{d}^2\rho}{\iint_{-\infty}^{\infty}S_x(\boldsymbol{\rho})\mathrm{d}^2\rho + \iint_{-\infty}^{\infty}S_y(\boldsymbol{\rho})\mathrm{d}^2\rho}$$
$$+ \frac{\iint_{-\infty}^{\infty}(x-\langle x\rangle)^2 S_y(\boldsymbol{\rho})\mathrm{d}^2\rho}{\iint_{-\infty}^{\infty}S_x(\boldsymbol{\rho})\mathrm{d}^2\rho + \iint_{-\infty}^{\infty}S_y(\boldsymbol{\rho})\mathrm{d}^2\rho}$$
$$\sigma_{f_x}^2 = \frac{\iint_{-\infty}^{\infty}(f_x-\langle f_x\rangle)^2 \mathrm{Tr}[\underline{\tilde{\mathbf{W}}}(\mathbf{f},\mathbf{f})]\mathrm{d}^2 f}{\iint_{-\infty}^{\infty}\mathrm{Tr}[\underline{\tilde{\mathbf{W}}}(\mathbf{f},\mathbf{f})]\mathrm{d}^2 f}$$
$$= \frac{\iint_{-\infty}^{\infty}(f_x-\langle f_x\rangle)^2 \tilde{S}_x(\mathbf{f})\mathrm{d}^2 f}{\iint_{-\infty}^{\infty}\tilde{S}_x(\mathbf{f})\mathrm{d}^2 f + \iint_{-\infty}^{\infty}\tilde{S}_y(\mathbf{f})\mathrm{d}^2 f}$$
$$+ \frac{\iint_{-\infty}^{\infty}(f_x-\langle f_x\rangle)^2 \tilde{S}_y(\mathbf{f})\mathrm{d}^2 f}{\iint_{-\infty}^{\infty}\tilde{S}_x(\mathbf{f})\mathrm{d}^2 f + \iint_{-\infty}^{\infty}\tilde{S}_y(\mathbf{f})\mathrm{d}^2 f}, \tag{3}$$

where $\underline{\mathbf{W}}$ is the cross-spectral density (CSD) matrix[17,28,29] of the beam at its waist location, Tr is the trace, and $S_\alpha(\boldsymbol{\rho}) = W_{\alpha\alpha}(\boldsymbol{\rho},\boldsymbol{\rho})$ are the spectral densities (SDs)[17,28,29] of the beam's $\alpha = x, y$ polarization components.

Continuing to define the symbols in Eq. (3), $\underline{\tilde{\mathbf{W}}}$ is the Fourier transform of $\underline{\mathbf{W}}$, i.e.:

$$\underline{\tilde{\mathbf{W}}}(\mathbf{f}_1,\mathbf{f}_2) = \iiiint_{-\infty}^{\infty}\underline{\mathbf{W}}(\boldsymbol{\rho}_1,\boldsymbol{\rho}_2)\exp[-\mathrm{j}2\pi(\boldsymbol{\rho}_1\cdot\mathbf{f}_1 - \boldsymbol{\rho}_2\cdot\mathbf{f}_2)] \times \mathrm{d}^2\rho_1\,\mathrm{d}^2\rho_2, \tag{4}$$

where $\tilde{S}_\alpha$ is as follows:

$$\tilde{S}_\alpha(\mathbf{f}) = \iiiint_{-\infty}^{\infty}W_{\alpha\alpha}(\boldsymbol{\rho}_1,\boldsymbol{\rho}_2)\exp[-\mathrm{j}2\pi(\boldsymbol{\rho}_1-\boldsymbol{\rho}_2)\cdot\mathbf{f}] \times \mathrm{d}^2\rho_1\,\mathrm{d}^2\rho_2, \tag{5}$$

where $\boldsymbol{\rho} = \hat{\mathbf{x}}x + \hat{\mathbf{y}}y$ and $\mathbf{f} = \hat{\mathbf{x}}f_x + \hat{\mathbf{y}}f_y$. Note that the denominators of σ_x^2 and $\sigma_{f_x}^2$ are equal due to Parseval's theorem. As such, we define and use the symbol $P = P_x + P_y$ hereafter to represent this normalization factor.

Last, $\langle x\rangle$ and $\langle f_x\rangle$ are the normalized beam "first moments" at the beam's waist location and in the spatial frequency domain, respectively, such that

$$\langle x\rangle = \frac{\iint_{-\infty}^{\infty}xS_x(\boldsymbol{\rho})\mathrm{d}^2\rho}{P_x+P_y} + \frac{\iint_{-\infty}^{\infty}xS_y(\boldsymbol{\rho})\mathrm{d}^2\rho}{P_x+P_y}$$
$$\langle f_x\rangle = \frac{\iint_{-\infty}^{\infty}f_x\tilde{S}_x(\mathbf{f})\mathrm{d}^2 f}{P_x+P_y} + \frac{\iint_{-\infty}^{\infty}f_x\tilde{S}_y(\mathbf{f})\mathrm{d}^2 f}{P_x+P_y}. \tag{6}$$

Following the scalar partially coherent source analysis presented in Refs. 5 and 6, we choose the z axis—the mean propagation direction of the random beam—such that $\langle x\rangle = \langle f_x\rangle = 0$. This permits us to write Eq. (3) as follows:

$$\sigma_x^2 = \frac{P_x}{P_x+P_y}\sigma_{x,x}^2 + \frac{P_y}{P_x+P_y}\sigma_{x,y}^2$$
$$\sigma_{f_x}^2 = \frac{P_x}{P_x+P_y}\sigma_{f_x,x}^2 + \frac{P_y}{P_x+P_y}\sigma_{f_x,y}^2, \tag{7}$$

where $\sigma_{x,\alpha}^2$ and $\sigma_{f_x,\alpha}^2$ are as follows:

$$\sigma_{x,\alpha}^2 = \frac{1}{P_\alpha}\iint_{-\infty}^{\infty}x^2S_\alpha(\boldsymbol{\rho})\mathrm{d}^2\rho \quad \sigma_{f_x,\alpha}^2 = \frac{1}{P_\alpha}\iint_{-\infty}^{\infty}f_x^2\tilde{S}_\alpha(\mathbf{f})\mathrm{d}^2 f. \tag{8}$$

Substituting Eq. (7) into Eq. (2) and simplifying produce as follows:

$$M_x^4 = \frac{P_x}{(P_x+P_y)^2}\left(P_x + \frac{\sigma_{x,y}^2}{\sigma_{x,x}^2}P_y\right)[4\pi\sigma_{x,x}\sigma_{f_x,x}]^2 + \frac{P_y}{(P_x+P_y)^2}\left(P_y + \frac{\sigma_{x,x}^2}{\sigma_{x,y}^2}P_x\right)[4\pi\sigma_{x,y}\sigma_{f_x,y}]^2. \tag{9}$$

The bracketed quantities in Eq. (9) are the vector component beam quality factors, and therefore,

$$M_x^4 = \frac{1}{P_x+P_y}\left(\frac{P_x}{P_x+P_y}\sigma_{x,x}^2 + \frac{P_y}{P_x+P_y}\sigma_{x,y}^2\right) \times \left(\frac{P_x}{\sigma_{x,x}^2}M_{x,x}^4 + \frac{P_y}{\sigma_{x,y}^2}M_{x,y}^4\right), \tag{10}$$

where $M_{x,\alpha}^2 = 4\pi\sigma_{x,\alpha}\sigma_{f_x,\alpha}$ are the beam quality factors for the $\alpha = x, y$ vector components.

1.2 *Prior M_x^2 Scalar Analysis*

Through extensive analysis and clever mathematics, Refs. 5 and 6 showed that M_x^2 for a scalar beam of any state of coherence is as follows:

$$M_x^4 = 16\pi^2\sigma_x^2\sigma_{f_x}^2 - J^2, \tag{11}$$

where σ_x^2 is given in Eq. (8) but computed in the source plane, $\sigma_{f_x}^2$ is as follows:

$$\sigma_{f_x}^2 = \frac{1}{4\pi^2 P}\iint_{-\infty}^{\infty}\frac{\partial^2 W(\boldsymbol{\rho}_1,\boldsymbol{\rho}_2)}{\partial x_1\partial x_2}\bigg|_{\boldsymbol{\rho},\boldsymbol{\rho}}\mathrm{d}^2\rho \tag{12}$$

and J is

$$J = \frac{1}{P}\,\mathrm{Im}\left[\iint_{-\infty}^{\infty}f_x\frac{\partial\tilde{W}(\mathbf{f}_1,\mathbf{f}_2)}{\partial f_{1x}}\bigg|_{\mathbf{f},\mathbf{f}}\mathrm{d}^2 f\right]. \tag{13}$$

The $|_{\boldsymbol{\rho},\boldsymbol{\rho}}$ and $|_{\mathbf{f},\mathbf{f}}$ denote that $\boldsymbol{\rho}_1 = \boldsymbol{\rho}_2 = \boldsymbol{\rho}$ and $\mathbf{f}_1 = \mathbf{f}_2 = \mathbf{f}$ after computing the partial derivatives, respectively.

For Schell-model sources,[17,28] Ref. 6 showed that Eq. (11) further reduces to

$$M_x^4 = (M_x^c)^4 - 4\sigma_x^2\frac{\partial^2 a(\boldsymbol{\rho}_d)}{\partial x_d^2}\bigg|_{\boldsymbol{\rho}_d=0}, \tag{14}$$

where $(M_x^c)^2$ is the beam quality factor of the corresponding coherent source, $\boldsymbol{\rho}_d = \hat{\mathbf{x}}x_d + \hat{\mathbf{y}}y_d = \hat{\mathbf{x}}(x_1-x_2) + \hat{\mathbf{y}}(y_1-y_2)$, and $a(\boldsymbol{\rho}_d)$ is related to the source's spectral autocorrelation function by

$$\mu(\boldsymbol{\rho}_d) = a(\boldsymbol{\rho}_d)\exp[\mathrm{j}\psi(\boldsymbol{\rho}_d)]. \tag{15}$$

Both a and ψ are real functions. Since $\mu(0) = 1$ and $\mu(-\boldsymbol{\rho}_d) = \mu^*(\boldsymbol{\rho}_d)$, $a(0) = 1, \psi(0) = 0, a(-\boldsymbol{\rho}_d) = a(\boldsymbol{\rho}_d)$, and

$\psi(-\boldsymbol{\rho}_d) = -\psi(\boldsymbol{\rho}_d)$. If μ is real, then $a = \mu$, and μ can be substituted directly into Eq. (14).

1.3 *New M_x^2 Vector Analysis*

Substituting in Eq. (14) for the vector component beam quality factors in Eq. (10) and simplifying produce as follows:

$$M_x^4 = \frac{1}{P_x + P_y}\left[\frac{P_x}{P_x + P_y}\sigma_{x,x}^2 + \frac{P_y}{P_x + P_y}\sigma_{x,y}^2\right] \times \left\{\frac{P_x}{\sigma_{x,x}^2}\left[(M_{x,x}^{\mathrm{c}})^4 - 4\sigma_{x,x}^2\left.\frac{\partial^2 a_{xx}(\boldsymbol{\rho}_d)}{\partial x_d^2}\right|_{\boldsymbol{\rho}_d=0}\right] + \frac{P_x}{\sigma_{x,y}^2}\left[(M_{x,y}^{\mathrm{c}})^4 - 4\sigma_{x,y}^2\left.\frac{\partial^2 a_{yy}(\boldsymbol{\rho}_d)}{\partial x_d^2}\right|_{\boldsymbol{\rho}_d=0}\right]\right\}. \tag{16}$$

Because M_x^2 in Eq. (16) is expressed in terms of vector component quantities (i.e., $M_{x,\alpha}^{\mathrm{c}}$, $\sigma_{x,\alpha}^2$, P_α, and $a_{\alpha\alpha}$), it is easy to use, in practice, to calculate the beam quality factor. It is not, however, the most simplified or physical form. Noting that the bracketed quantity on the first line of Eq. (16) is equal to σ_x^2 via Eq. (7), expanding, and then simplifying Eq. (16) yields as follows:

$$M_x^4 = \sigma_x^2\left[\frac{P_x}{P_x+P_y}\frac{(M_{x,x}^{\mathrm{c}})^4}{\sigma_{x,x}^2} + \frac{P_y}{P_x+P_y}\frac{(M_{x,y}^{\mathrm{c}})^4}{\sigma_{x,y}^2}\right] - 4\sigma_x^2\left(\frac{P_x}{P_x+P_y}\left.\frac{\partial^2 a_{xx}(\boldsymbol{\rho}_d)}{\partial x_d^2}\right|_{\boldsymbol{\rho}_d=0} + \frac{P_y}{P_x+P_y}\left.\frac{\partial^2 a_{yy}(\boldsymbol{\rho}_d)}{\partial x_d^2}\right|_{\boldsymbol{\rho}_d=0}\right). \tag{17}$$

Last, substituting in $(M_{x,\alpha}^{\mathrm{c}})^2 = 4\pi\sigma_{x,\alpha}\sigma_{f_x,\alpha}^{\mathrm{c}}$, recalling Eq. (7), and simplifying, the desired result is obtained as follows:

$$\begin{aligned} M_x^4 &= (4\pi\sigma_x)^2\left[\frac{P_x}{P_x+P_y}(\sigma_{f_x,x}^{\mathrm{c}})^2 + \frac{P_y}{P_x+P_y}(\sigma_{f_x,y}^{\mathrm{c}})^2\right] - 4\sigma_x^2\left[\frac{P_x}{P_x+P_y}\left.\frac{\partial^2 a_{xx}(\boldsymbol{\rho}_d)}{\partial x_d^2}\right|_{\boldsymbol{\rho}_d=0} + \frac{P_y}{P_x+P_y}\left.\frac{\partial^2 a_{yy}(\boldsymbol{\rho}_d)}{\partial x_d^2}\right|_{\boldsymbol{\rho}_d=0}\right] \\ &= (M_x^{\mathrm{c}})^4 - 4\sigma_x^2\left[\frac{P_x}{P_x+P_y}\left.\frac{\partial^2 a_{xx}(\boldsymbol{\rho}_d)}{\partial x_d^2}\right|_{\boldsymbol{\rho}_d=0} + \frac{P_y}{P_x+P_y}\left.\frac{\partial^2 a_{yy}(\boldsymbol{\rho}_d)}{\partial x_d^2}\right|_{\boldsymbol{\rho}_d=0}\right]. \end{aligned} \tag{18}$$

Equation (18)—in particular, the last line of Eq. (18)—is the main analytical result of this paper and generalizes the scalar result presented in Ref. 6. Its form is very similar to the scalar result in that M_x^2 depends on the coherence of the source only through the second derivatives of the vector correlation functions evaluated at $\boldsymbol{\rho}_d = 0$. Rather intuitively, it differs in the fact that the "coherence contributions," σ_x and $\sigma_{f_x}^{\mathrm{c}}$, are weighted by the fraction of power in the associated vector component. This being the case, one is tempted to try to manipulate Eq. (18) into the sum of weighted, component, beam quality factors $M_{x,\alpha}^2$. Unfortunately, this simple, physical form for M_x^2 is spoiled by cross terms, which are evident in Eq. (16).

1.4 *Examples*

Here, we calculate the M_x^2 for two example, vector Schell-model sources. We then simulate them in terms of M_x^2 in Sec. 2.

1.4.1 *EM Gaussian Schell-model source*

The elements of the CSD matrix for an EGSM source are as follows:

$$W_{\alpha\beta}(\boldsymbol{\rho}_1, \boldsymbol{\rho}_2) = A_\alpha \exp\left(-\frac{\rho_1^2}{4\sigma_\alpha^2}\right) A_\beta \exp\left(-\frac{\rho_2^2}{4\sigma_\beta^2}\right) \times B_{\alpha\beta} \exp\left(-\frac{|\boldsymbol{\rho}_1 - \boldsymbol{\rho}_2|^2}{2\delta_{\alpha\beta}^2}\right), \tag{19}$$

where $\alpha, \beta = x, y$, A_α is the amplitude of the α field component, and σ_α is the RMS width of the α component SD. Also in Eq. (19), $B_{\alpha\beta}$ is the complex correlation coefficient between the α and β field components and $\delta_{\alpha\beta}$ is the RMS width of the cross-correlation function $\mu_{\alpha\beta}$, i.e., the cross-correlation function of the α and β field components.[17,29] The EGSM source parameters—A_α, σ_α, $\delta_{\alpha\beta}$, and $B_{\alpha\beta}$—must satisfy the realizability conditions derived in Refs. 17 and 30. Since only the diagonal elements of the CSD matrix are required to compute M_x^2, the $B_{\alpha\alpha} = 1$ criterion is the most relevant here.

To compute M_x^2, we use Eq. (16). The normalized beam widths of the x and y components of the EGSM source, computed using Eq. (8), are $\sigma_{x,\alpha} = \sigma_\alpha$. The powers in the x and y components of the source are computed using the denominators in Eq. (3) and are $P_\alpha = 2\pi\sigma_\alpha^2 A_\alpha^2$. The corresponding coherent source to the EGSM source defined in Eq. (19) is as follows:

$$W_{\alpha\beta}^{\mathrm{c}}(\boldsymbol{\rho}_1, \boldsymbol{\rho}_2) = A_\alpha A_\beta B_{\alpha\beta} \exp\left(-\frac{\rho_1^2}{4\sigma_\alpha^2}\right) \exp\left(-\frac{\rho_2^2}{4\sigma_\beta^2}\right). \tag{20}$$

This CSD function describes a vector source composed of horizontally and vertically polarized, spatially coherent, correlated, Gaussian beams. Since the x and y vector components of the source are Gaussian beams, the component beam quality factors are $(M_{x,\alpha}^{\mathrm{c}})^2 = 1$. Last, the component spectral correlation functions $\mu_{\alpha\alpha}$ are real; therefore, $a_{\alpha\alpha} = \mu_{\alpha\alpha}$ and the second derivatives in Eq. (16) evaluate to

$$\left.\frac{\partial^2 a_{\alpha\alpha}(\boldsymbol{\rho}_d)}{\partial x_d^2}\right|_{\boldsymbol{\rho}_d=0} = \left.\frac{\partial^2}{\partial x_d^2}\exp\left(-\frac{\rho_d^2}{2\delta_{\alpha\alpha}^2}\right)\right|_{\boldsymbol{\rho}_d=0} = -\frac{1}{\delta_{\alpha\alpha}^2}. \tag{21}$$

Substituting the quantities discussed in the previous paragraph into Eq. (16) and simplifying produce as follows:

$$M_x^2 = \sqrt{\frac{A_x^2\sigma_x^4 + A_y^2\sigma_y^4}{(A_x^2\sigma_x^2 + A_y^2\sigma_y^2)^2}}\left[A_x^2\left(1 + 4\frac{\sigma_x^2}{\delta_{xx}^2}\right) + A_y^2\left(1 + 4\frac{\sigma_y^2}{\delta_{yy}^2}\right)\right]^{1/2}. \tag{22}$$

This expression is equal to the M_x^2 for an EGSM source derived in Refs. 9–12 using different methods. Note that letting either $A_x = 0$ or $A_y = 0$ yields the M_x^2 for a scalar GSM source first derived in Ref. 6. We generate an EGSM source with a specified M_x^2 in Sec. 2.

1.4.2 *Vector optical coherence lattices*

Another popular and relatively new example of a vector partially coherent source is the so-called vector optical coherence lattice (VOCL).[14] The CSD matrix elements for a VOCL take the form:

$$W_{\alpha\beta}(\boldsymbol{\rho}_1,\boldsymbol{\rho}_2)=A_\alpha \exp\left(-\frac{\rho_1^2}{4\sigma_\alpha^2}\right)A_\beta \exp\left(-\frac{\rho_2^2}{4\sigma_\beta^2}\right) \times B_{\alpha\beta}\text{jinc}\left(\frac{|\boldsymbol{\rho}_1-\boldsymbol{\rho}_2|}{\sqrt{2}\delta_{\alpha\beta}}\right)\frac{1}{N}\sum_{n=1}^{N}\exp[-\text{j}\mathbf{v}_n\cdot(\boldsymbol{\rho}_1-\boldsymbol{\rho}_2)], \tag{23}$$

where $\text{jinc}(x)=2J_1(x)/x$, J_1 is a first-order Bessel function of the first kind, and $\mathbf{v}_n=\hat{\mathbf{x}}v_{nx}+\hat{\mathbf{y}}v_{ny}$ is a vector that points from the origin to the n'th node of the "coherence lattice." The other symbols have been defined previously and generally have the same physical interpretation as the EGSM source. One should immediately recognize that the spectral cross-correlation function in Eq. (23) is equivalent to the FZ pattern (spatial Fourier transform) of an array of circular transmitters.

To find the beam quality factor, we again use Eq. (16). The $\sigma_{x,\alpha}=\sigma_\alpha$, $P_\alpha=2\pi\sigma_\alpha^2A_\alpha^2$, and $(M_{x,\alpha}^{\text{c}})^2=1$ are the same as in the EGSM source example. The second derivative of $a_{\alpha\alpha}$ is much more difficult. Here, for analytical convenience, we assume that the lattice nodes are symmetric about the origin. This assumption means that $\mu_{\alpha\alpha}$ is real, and thus, $a_{\alpha\alpha}=\mu_{\alpha\alpha}$. After much calculus and algebra (details in Sec. 4 Appendix A), the second derivatives in Eq. (16) evaluate to

$$\left.\frac{\partial^2 a_{\alpha\alpha}(\boldsymbol{\rho}_d)}{\partial x_d^2}\right|_{\boldsymbol{\rho}_d=0}=\left.\frac{\partial^2}{\partial x_d^2}\left[\text{jinc}\left(\frac{\rho_d}{\sqrt{2}\delta_{\alpha\alpha}}\right)\frac{1}{N}\sum_{n=1}^{N}\exp(-\text{j}\mathbf{v}_n\cdot\boldsymbol{\rho}_d)\right]\right|_{\boldsymbol{\rho}_d=0} =-\frac{1}{8\delta_{\alpha\alpha}^2}-\frac{1}{N}\sum_{n=1}^{N}v_{nx}^2. \tag{24}$$

Substituting $\sigma_{x,\alpha}=\sigma_\alpha$, $P_\alpha=2\pi\sigma_\alpha^2A_\alpha^2$, $(M_{x,\alpha}^{\text{c}})^2=1$; Eq. (24) into Eq. (16); and simplifying produce as follows:

$$M_x^2=\sqrt{\frac{A_x^2\sigma_x^4+A_y^2\sigma_y^4}{(A_x^2\sigma_x^2+A_y^2\sigma_y^2)^2}} \times\left\{A_x^2\left[1+\frac{1}{2}\frac{\sigma_x^2}{\delta_{xx}^2}\left(1+\frac{8}{N}\sum_{n=1}^{N}\delta_{xx}^2v_{nx}^2\right)\right] +A_y^2\left[1+\frac{1}{2}\frac{\sigma_y^2}{\delta_{yy}^2}\left(1+\frac{8}{N}\sum_{n=1}^{N}\delta_{yy}^2v_{nx}^2\right)\right]\right\}^{1/2}. \tag{25}$$

We generate and analyze a VOCL, in terms of M_x^2, in Sec. 2.

1.5 *Generating Stochastic Vector Fields in Terms of M_x^2*

An instance of a Schell-model source can be generated by filtering a two-dimensional (2-D) array of circular complex Gaussian random numbers. For computational efficiency, it is best to perform the filtering in the spectral domain using the convolution theorem. This process has been described in the literature many times.[31–37] Here, we present the necessary equations to implement the technique.

Any type of vector Schell-model source can be formed by the following optical field realization:[31,33]

$$E_\alpha(\boldsymbol{\rho})=C_\alpha\exp\left(-\frac{\rho^2}{4\sigma_\alpha^2}\right)T_\alpha(\boldsymbol{\rho}), \tag{26}$$

where C_α is the complex amplitude and T_α is the stochastic complex transmittance screen for the $\alpha=x,y$ component of the field, respectively. T_α is formed from correlated, circular complex Gaussian random numbers. Here, we have assumed a Gaussian shape for the source, considering that Sec. 1.4 examples also have Gaussian shapes. In general, the source can take any shape.

Hereafter, we specialize the mathematics to generate the sources discussed in Sec. 1.4. The procedure for synthesizing any other type of vector Schell-model source is the same as presented here, only the mathematical details change.

Taking the cross-correlation of Eq. (26) with E_β and comparing the resulting expression to Eqs. (19) and (23) yields the following equalities: $|C_\alpha|=A_\alpha$, $\arg(C_\alpha)-\arg(C_\beta)=\arg(B_{\alpha\beta})$, and

$$\langle T_\alpha(\boldsymbol{\rho}_1)T_\beta^*(\boldsymbol{\rho}_2)\rangle=\begin{cases}|B_{\alpha\beta}|\exp\left(-\frac{|\boldsymbol{\rho}_1-\boldsymbol{\rho}_2|^2}{2\delta_{\alpha\beta}^2}\right) & \text{EGSM source}\\ |B_{\alpha\beta}|\text{jinc}\left(\frac{|\boldsymbol{\rho}_1-\boldsymbol{\rho}_2|}{\sqrt{2}\delta_{\alpha\beta}}\right)\frac{1}{N}\sum_{n=1}^{N}\exp[-\text{j}\mathbf{v}_n\cdot(\boldsymbol{\rho}_1-\boldsymbol{\rho}_2)] & \text{VOCL}\end{cases}. \tag{27}$$

Because potentially $|B_{xy}|>0$, T_x and T_y, in general, must be generated from correlated Gaussian random numbers. To see this and reveal the conditions on the values of $|B_{xy}|$ and δ_{xy}, we note that an instance of T_α is generated by[31,32]

$$T_\alpha[i,j]=\sum_m\sum_n r_\alpha[m,n]\sqrt{\frac{\Phi_{T_\alpha}[m,n]}{2L_xL_y}}\exp\left(\text{j}\frac{2\pi}{N_x}mi\right) \times\exp\left(\text{j}\frac{2\pi}{N_y}nj\right), \tag{28}$$

where N_x, N_y are the numbers of grid points in the x, y directions, $L_x=N_x\Delta$, $L_y=N_y\Delta$ are the lengths of the grid in the x, y directions in meters, and Δ is the grid spacing. In Eq. (28), r_α is an $N_y\times N_x$ grid of zero-mean, unit-variance circular complex Gaussian random numbers and Φ_{T_α} is the spatial power spectrum of T_α, i.e., the Fourier transform of the autocorrelation of T_α. For the examples discussed in Sec. 1.4:

$$\Phi_{T_\alpha}(\mathbf{f})=\begin{cases}2\pi\delta_{\alpha\alpha}^2\exp(-2\pi^2\delta_{\alpha\alpha}^2f^2) & \text{EGSM source}\\ 8\pi\delta_{\alpha\alpha}^2\frac{1}{N}\sum_{n=1}^{N}\text{circ}\left(\sqrt{8}\pi\delta_{\alpha\alpha}\left|\mathbf{f}+\frac{\mathbf{v}_n}{2\pi}\right|\right) & \text{VOCL}\end{cases}, \tag{29}$$

where $\mathrm{circ}(x)$ is the circle function defined in Ref. 38. We note that Eq. (28) is in the form of a discrete, inverse Fourier transform; thus, T_α can be generated quickly and efficiently using the fast Fourier transform algorithm.

Using Eqs. (28) and (29), a T_α with a specified $\delta_{\alpha\alpha}$ is produced. Physically, this leads to an EGSM source or VOCL with the correct, diagonal, CSD matrix elements. Recall that M_x^2 depends only on these elements, and therefore, one could ignore any correlation between the x and y vector components (i.e., produce instances of T_x and T_y from independent Gaussian random numbers) and still produce a beam with the desired M_x^2. Doing this step results in a beam that is randomly, partially, or fully linearly polarized.

To generate a vector Schell-model source with a general polarization state, one must control the off-diagonal elements of the CSD matrix as well. This requires examination of the cross-correlation of T_x with T_y, namely,

$$\begin{aligned}\langle T_x[i_1,j_1]T_y^*[i_2,j_2]\rangle = &\sum_{m_1}\sum_{n_1}\sum_{m_2}\sum_{n_2}\frac{\langle r_x[m_1,n_1]r_y^*[m_2,n_2]\rangle}{2L_xL_y}\\ &\times\sqrt{\Phi_{T_x}[m_1,n_1]\Phi_{T_y}[m_2,n_2]}\\ &\times\exp\left(\mathrm{j}\frac{2\pi}{N_x}m_1i_1\right)\exp\left(\mathrm{j}\frac{2\pi}{N_y}n_1j_1\right)\\ &\times\exp\left(-\mathrm{j}\frac{2\pi}{N_x}m_2i_2\right)\exp\left(-\mathrm{j}\frac{2\pi}{N_y}n_2j_2\right).\end{aligned} \tag{30}$$

The moment $\langle r_x[m_1,n_1]r_y^*[m_2,n_2]\rangle = 2\Gamma\delta[m_1-m_2]\delta[n_1-n_2]$, where Γ is the correlation coefficient between the r_x and r_y random numbers and $\delta[n]$ is the discrete Dirac delta function. Substituting this into Eq. (30) and simplifying produce as follows:

$$\begin{aligned}\langle T_x[i_1,j_1]T_y^*[i_2,j_2]\rangle = &\sum_m\sum_n\Gamma\sqrt{\Phi_{T_x}[m,n]\Phi_{T_y}[m,n]}\\ &\times\frac{1}{L_xL_y}\exp\left[\mathrm{j}\frac{2\pi}{N_x}m(i_1-i_2)\right]\exp\left[\mathrm{j}\frac{2\pi}{N_y}n(j_1-j_2)\right].\end{aligned} \tag{31}$$

The $\Gamma\sqrt{\Phi_{T_x}\Phi_{T_y}}$ must equal the cross-power spectra, or the Fourier transforms of the expressions in Eq. (27), viz.,

$$\Phi_{T_xT_y}(\mathbf{f}) = \begin{cases}|B_{xy}|2\pi\delta_{xy}^2\exp(-2\pi^2\delta_{xy}^2f^2) & \text{EGSM source}\\ |B_{xy}|8\pi\delta_{xy}^2\frac{1}{N}\sum_{n=1}^N\mathrm{circ}\left(\sqrt{8}\pi\delta_{xy}\left|\mathbf{f}+\frac{\mathbf{v}_n}{2\pi}\right|\right) & \text{VOCL}\end{cases}. \tag{32}$$

This step produces the following relation for EGSM sources:

$$\begin{aligned}&\Gamma\delta_{xx}\delta_{yy}\exp\left[-2\pi^2\left(\frac{\delta_{xx}^2+\delta_{yy}^2}{2}\right)f^2\right]\\ &\quad=|B_{xy}|\delta_{xy}^2\exp(-2\pi^2\delta_{xy}^2f^2).\end{aligned} \tag{33}$$

From here, it is quite clear that

$$\delta_{xy}=\sqrt{\frac{\delta_{xx}^2+\delta_{yy}^2}{2}}\quad |B_{xy}|=\Gamma\frac{2\delta_{xx}\delta_{yy}}{\delta_{xx}^2+\delta_{yy}^2}, \tag{34}$$

where $0\le\Gamma\le1$. These conditions were first derived in Ref. 31.

The VOCL conditions on $|B_{xy}|$ and δ_{xy} are derived from

$$\begin{aligned}&\Gamma\prod_{\alpha=x,y}\left[\delta_{\alpha\alpha}^2\sum_{n=1}^N\mathrm{circ}\left(\sqrt{8}\pi\delta_{\alpha\alpha}\left|\mathbf{f}-\frac{\mathbf{v}_n}{2\pi}\right|\right)\right]^{1/2}\\ &=|B_{xy}|\delta_{xy}^2\sum_{n=1}^N\mathrm{circ}\left(\sqrt{8}\pi\delta_{xy}\left|\mathbf{f}-\frac{\mathbf{v}_n}{2\pi}\right|\right).\end{aligned} \tag{35}$$

Because of this expression, it is not likely that conditions similar to Eq. (34) can be derived for a VOCL. Two rather trivial, but physically important conditions can be derived by letting $\Gamma=|B_{xy}|$:

1. If $B_{xy}=0$, δ_{xy} is physically meaningless and its value is irrelevant, T_x and T_y are statistically independent, and $\delta_{\alpha\alpha}$ can be chosen freely. This produces a VOCL with a diagonal CSD matrix and the beam is randomly, partially, or fully linearly polarized.
2. If $|B_{xy}|\neq0$, then $\delta_{xx}=\delta_{yy}=\delta_{xy}$, and T_x and T_y are correlated to some degree. This produces a VOCL with a full CSD matrix and the beam is, most generally, elliptically partially polarized.

These same conditions apply to many other vector Schell-model sources, e.g., EM multi-Gaussian Schell-model[17,21] and EM Bessel-Gaussian Schell-model sources.[22,32]

The last step is to express the EGSM source and VOCL conditions derived above in terms of M_x^2. The EGSM source and VOCL component beam quality factors are as follows:

$$M_{x,\alpha}^4=\begin{cases}1+4\frac{\sigma_\alpha^2}{\delta_{\alpha\alpha}^2} & \text{EGSM source}\\ 1+\frac{1}{2}\frac{\sigma_\alpha^2}{\delta_{\alpha\alpha}^2}\left(1+\frac{8}{N}\sum_{n=1}^N\delta_{\alpha\alpha}^2v_{nx}^2\right) & \text{VOCL}\end{cases}. \tag{36}$$

Referring back to Eqs. (22) and (25), substituting Eq. (36) into those expressions and inverting produces as follows:

$$M_x^4\frac{(A_x^2\sigma_x^2+A_y^2\sigma_y^2)^2}{A_x^2\sigma_x^4+A_y^2\sigma_y^4}=A_x^2M_{x,x}^4+A_y^2M_{x,y}^4. \tag{37}$$

We assume that A_α and σ_α are given. This makes sense as we would expect the on-axis intensity A_α^2 and size of the source to be known. In addition, since generally $M_{x,x}^2\neq M_{x,y}^2$ (or equivalently, $\delta_{xx}\neq\delta_{yy}$), one of those must be given. Without loss of generality, we assume $M_{x,y}^2$ is known. Simplifying Eq. (37) further produces as follows:

$$M_{x,x}^4=\frac{1}{A_x^2}\left[M_x^4\frac{(A_x^2\sigma_x^2+A_y^2\sigma_y^2)^2}{A_x^2\sigma_x^4+A_y^2\sigma_y^4}-A_y^2M_{x,y}^4\right]. \tag{38}$$

Last, substituting Eq. (36) into Eq. (38) and simplifying yields

$$\delta_{xx}^2 = 4A_x^2\sigma_x^2(A_x^2\sigma_x^4 + A_y^2\sigma_y^4)\Bigg\{(A_x^2\sigma_x^2 + A_y^2\sigma_y^2)^2M_x^4 - (A_x^2\sigma_x^4 + A_y^2\sigma_y^4)\left[A_x^2 + A_y^2\left(1 + 4\frac{\sigma_y^2}{\delta_{yy}^2}\right)\right]\Bigg\}^{-1} \tag{39}$$

for an EGSM source, and

$$\delta_{xx}^2 = \frac{1}{2}A_x^2\sigma_x^2(A_x^2\sigma_x^4 + A_y^2\sigma_y^4)\Bigg\{(A_x^2\sigma_x^2 + A_y^2\sigma_y^2)^2M_x^4 - (A_x^2\sigma_x^4 + A_y^2\sigma_y^4)\left[A_x^2\left(1 + 4\frac{\sigma_x^2}{N}\sum_{n=1}^{N}v_{nx}^2\right) + A_y^2\left(1 + 4\frac{\sigma_y^2}{N}\sum_{n=1}^{N}v_{nx}^2 + \frac{1}{2}\frac{\sigma_y^2}{\delta_{yy}^2}\right)\right]\Bigg\}^{-1} \tag{40}$$

for a VOCL. We note that the locations of the coherence lattice nodes $\mathbf{v}_n$ must be known to find δ_{xx}.

In summary, to produce an EGSM source or VOCL with a desired M_x^2:

1. Specify A_x, σ_x, A_y, σ_y, M_x^2, $M_{x,y}^2$ and for a VOCL, $\mathbf{v}_n$. Recall that $|C_\alpha| = A_\alpha$. The values of $M_{x,y}^2$, σ_y, and $\mathbf{v}_n$ (for a VOCL) determine δ_{yy} [see Eq. (36)].
2. Use Eq. (39) for an EGSM source or Eq. (40) for a VOCL to find δ_{xx}. For both sources, this effectively sets δ_{xy} [see Eq. (34) and VOCL conditions immediately following Eq. (35)].
3. Specify $\arg(C_x)$, $\arg(C_y)$, and $|B_{xy}|$. Recall that $\arg(C_x) - \arg(C_y) = \arg(B_{xy})$. For both sources, the value of $|B_{xy}|$ determines Γ [see Eq. (34) and for a VOCL, $\Gamma = |B_{xy}|$].
4. Use a multivariate Gaussian random number generator to produce correlated r_x and r_y. The means and covariance matrix are as follows:

$$\begin{aligned}
&\langle r_x^{\mathrm{r}}\rangle = \langle r_x^{\mathrm{i}}\rangle = \langle r_y^{\mathrm{r}}\rangle = \langle r_y^{\mathrm{i}}\rangle = 0\\
&\Sigma = \begin{bmatrix} \langle (r_x^{\mathrm{r}})^2\rangle & \langle r_x^{\mathrm{r}}r_x^{\mathrm{i}}\rangle & \langle r_x^{\mathrm{r}}r_y^{\mathrm{r}}\rangle & \langle r_x^{\mathrm{r}}r_y^{\mathrm{i}}\rangle \\ \langle r_x^{\mathrm{i}}r_x^{\mathrm{r}}\rangle & \langle (r_x^{\mathrm{i}})^2\rangle & \langle r_x^{\mathrm{i}}r_y^{\mathrm{r}}\rangle & \langle r_x^{\mathrm{i}}r_y^{\mathrm{i}}\rangle \\ \langle r_y^{\mathrm{r}}r_x^{\mathrm{r}}\rangle & \langle r_y^{\mathrm{r}}r_x^{\mathrm{i}}\rangle & \langle (r_y^{\mathrm{r}})^2\rangle & \langle r_y^{\mathrm{r}}r_y^{\mathrm{i}}\rangle \\ \langle r_y^{\mathrm{i}}r_x^{\mathrm{r}}\rangle & \langle r_y^{\mathrm{i}}r_x^{\mathrm{i}}\rangle & \langle r_y^{\mathrm{i}}r_y^{\mathrm{r}}\rangle & \langle (r_y^{\mathrm{i}})^2\rangle \end{bmatrix}\\
&\quad = \begin{bmatrix} 1 & 0 & \Gamma & 0 \\ 0 & 1 & 0 & \Gamma \\ \Gamma & 0 & 1 & 0 \\ 0 & \Gamma & 0 & 1 \end{bmatrix},\\
&r_x = r_x^{\mathrm{r}} + \mathrm{j}r_x^{\mathrm{i}}\\
&r_y = r_y^{\mathrm{r}} + \mathrm{j}r_y^{\mathrm{i}}
\end{aligned} \tag{41}$$

   where the superscripts "r" and "i" stand for real and imaginary parts, respectively.
5. Use Eqs. (28) and (29), the values of δ_{xx}, δ_{yy}, and $\mathbf{v}_n$ (for a VOCL), and the r_x and r_y from step 4 to generate instances of T_x and T_y.
6. Use Eq. (26), the values of C_x, C_y, σ_x, σ_y, and the T_x and T_y generated in step 5 to create an EGSM or VOCL field instance.

Since the generated fields are stochastic, this procedure will produce an EGSM source or VOCL with a desired, "on-average" M_x^2.

2 Simulation

Here, we present simulation results to validate the analysis in the previous section. We also examine the convergence of the stochastic vector fields to the desired M_x^2. Before presenting the results, we discuss the details of the setup.

2.1 *Setup*

For these Monte Carlo simulations, we used computational grids with $N_y = N_x = 512$ points per side. The grid spacings were chosen such that $\Delta = \min\{\sigma_x, \sigma_y\}/10$ resulting in 3 and 0.97 mm for the EGSM source and VOCL simulations, respectively. These spacings easily satisfied the Nyquist sampling criterion derived for Gaussian signals in Ref. 39. The EGSM source and VOCL parameters are given in Table 1. For the VOCL, the coherence lattice was rectangular with 5 rows and 4 columns of nodes spaced 500 m^{-1} apart.

We generated 20,000 EGSM source and VOCL field instances. From these, we computed the near-zone (NZ) (i.e., source plane) and FZ Stokes parameters, M_x^2, and M_y^2. The Stokes parameters in terms of the CSD matrix elements are as follows:[17,29]

$$\begin{aligned}
S_0(\boldsymbol{\rho}) &= W_{xx}(\boldsymbol{\rho},\boldsymbol{\rho}) + W_{yy}(\boldsymbol{\rho},\boldsymbol{\rho})\\
S_1(\boldsymbol{\rho}) &= W_{xx}(\boldsymbol{\rho},\boldsymbol{\rho}) - W_{yy}(\boldsymbol{\rho},\boldsymbol{\rho})\\
S_2(\boldsymbol{\rho}) &= W_{xy}(\boldsymbol{\rho},\boldsymbol{\rho}) + W_{yx}(\boldsymbol{\rho},\boldsymbol{\rho})\\
S_3(\boldsymbol{\rho}) &= \mathrm{j}[W_{yx}(\boldsymbol{\rho},\boldsymbol{\rho}) - W_{xy}(\boldsymbol{\rho},\boldsymbol{\rho})].
\end{aligned} \tag{42}$$

Table 1 EGSM source and VOCL parameters.

	EGSM	VOCL
A_x	1.3	1
A_y	1	1.7
σ_x	5 cm	1 cm
σ_y	3 cm	0.97 cm
B_{xy}	$0.15\exp(-\mathrm{j}\pi/6)$	0
M_x^2	10	11.4
M_y^2	10	14.2028
$M_{x,x}^2$	11	12.5
$M_{x,y}^2$	5.1446	10.9880
δ_{xx}	0.9129 cm	0.1286 cm
δ_{yy}	1.1889 cm	0.4707 cm
δ_{xy}	1.0599 cm	N/A

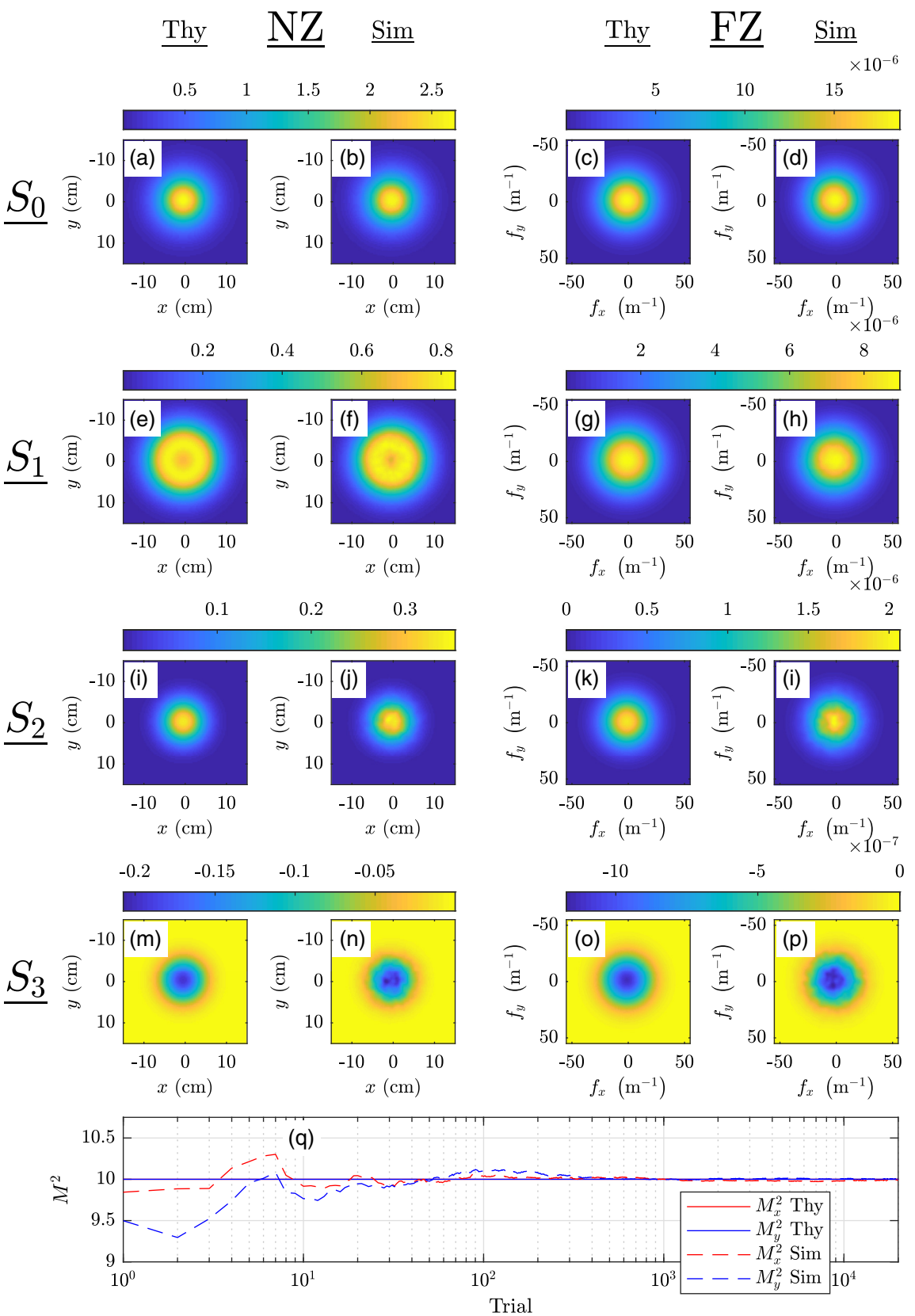

Fig. 1 EGSM source results—(a) S_0^{NZ} Thy, (b) S_0^{NZ} Sim, (c) S_0^{FZ} Thy, (d) S_0^{FZ} Sim, (e) S_1^{NZ} Thy, (f) S_1^{NZ} Sim, (g) S_1^{FZ} Thy, (h) S_1^{FZ} Sim, (i) S_2^{NZ} Thy, (j) S_2^{NZ} Sim, (k) S_2^{FZ} Thy, (l) S_2^{FZ} Sim, (m) S_3^{NZ} Thy (n) S_3^{NZ} Sim, (o) S_3^{FZ} Thy, (p) S_3^{FZ} Sim, and (q) convergence of simulated M_x^2 and M_y^2 to the corresponding theoretical values versus trial number.

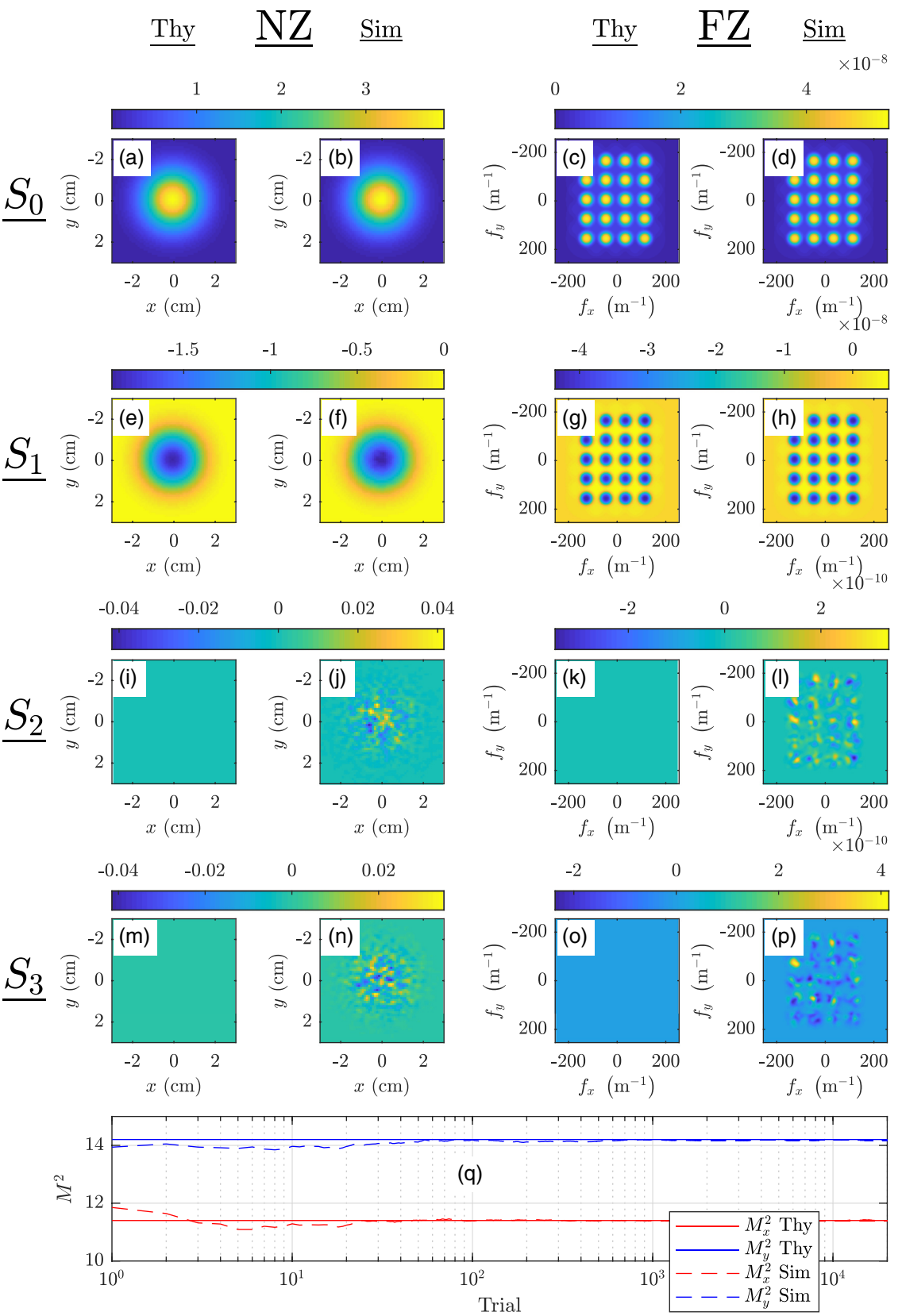

Fig. 2 VOCL results—(a) S_0^{NZ} Thy, (b) S_0^{NZ} Sim, (c) S_0^{FZ} Thy, (d) S_0^{FZ} Sim, (e) S_1^{NZ} Thy, (f) S_1^{NZ} Sim, (g) S_1^{FZ} Thy, (h) S_1^{FZ} Sim, (i) S_2^{NZ} Thy, (j) S_2^{NZ} Sim, (k) S_2^{FZ} Thy, (l) S_2^{FZ} Sim, (m) S_3^{NZ} Thy (n) S_3^{NZ} Sim, (o) S_3^{FZ} Thy, (p) S_3^{FZ} Sim, and (q) convergence of simulated M_x^2 and M_y^2 to the corresponding theoretical values versus trial number.

For M_x^2 and M_y^2, the σ_x, σ_{f_x}, σ_y, and σ_{f_y} [see Eq. (3)] were computed using trapezoidal numerical integration.

To verify that, we produced a source with the correct NZ and FZ polarization properties, we compared the simulated Stokes parameters with the corresponding theoretical quantities. The theoretical expressions for the EGSM source and VOCL NZ Stokes parameters were computed using Eqs. (19) and (23) and the values in Table 1, respectively. We computed the theoretical FZ Stokes parameters using those same equations and the Fourier transform in Eq. (4) resulting in

$$\tilde{W}_{\alpha\beta}(\mathbf{f},\mathbf{f}) = \begin{cases} A_\alpha A_\beta B_{\alpha\beta} \frac{16\pi^2\sigma_\alpha^2\sigma_\beta^2\delta_{\alpha\beta}^2}{2\sigma_\alpha^2+2\sigma_\beta^2+\delta_{\alpha\beta}^2} \exp\left[-\frac{4\pi^2\delta_{\alpha\beta}^2(\sigma_\alpha^2+\sigma_\beta^2)}{2\sigma_\alpha^2+2\sigma_\beta^2+\delta_{\alpha\beta}^2} f^2\right] & \text{EGSM source} \\ A_\alpha A_\beta B_{\alpha\beta} \frac{32\pi^2\sigma_\alpha^2\sigma_\beta^2\delta_{\alpha\beta}^2}{\sigma_\alpha^2+\sigma_\beta^2} \int_0^\infty \exp\left[-\frac{\delta_{\alpha\beta}^2}{2(\sigma_\alpha^2+\sigma_\beta^2)} u^2\right] & \\ \times J_1(u) \frac{1}{N}\sum_{n=1}^N J_0\left(\sqrt{8}\pi\delta_{\alpha\beta}\left|\mathbf{f}+\frac{\mathbf{v}_n}{2\pi}\right|u\right) \mathrm{d}u & \text{VOCL} \end{cases} . \tag{43}$$

The integral in the VOCL $\tilde{W}_{\alpha\beta}$ can be evaluated in closed form using Mellin transform techniques.[40] The resulting expression is an infinite series of hypergeometric functions.[41] Computing the result using this analytical relation is very slow; therefore, we evaluated the integral directly using numerical quadrature.

2.2 *Results*

Figures 1 and 2 show the EGSM source and VOCL results, respectively. The figures are organized as follows: the Stokes parameters are displayed in the first four rows—S_0, S_1, S_2, and S_3, respectively. The first two columns show the NZ results, with column 1 (the left column) showing the theoretical (Thy) results and column 2 (the right column) showing the simulated (Sim) results. Columns 3 and 4 show the FZ results, with an identical left-right arrangement of Thy (column 3) and Sim (column 4) results. Note that we have added row and column headings to Figs. 1 and 2 to aid the reader. Last, the fifth rows [Figs. 1(q) and 2(q)] show the convergence of the simulated M_x^2 and M_y^2 to the corresponding theoretical values versus Monte Carlo trial number.

Overall, the agreement between simulation and theory is excellent. We note that the visually conspicuous differences between the S_2 and S_3 Thy and Sim VOCL results in Fig. 2 are in fact quantitatively small (see the associated color bars above the subfigures). These discrepancies arise because of our choice of color scale and Thy $S_2 = S_3 = 0$. Running more Monte Carlo trials would reduce these errors; however, S_2 and S_3 Sim will never be identically zero for that would require an infinite number of trials.

The simulated M_x^2 and M_y^2 converge to the desired values in approximately 1,000 trials. This finding is consistent with the scalar Schell-model beam results in Ref. 27. Figures 1 and 2 validate the theoretical analysis presented in Sec. 1.

3 Conclusion

Here, we derived the M^2 factor for a general vector Schell-model beam. Starting with Siegman's M^2 definition, we found an expression for the M^2 factor of a vector partially coherent beam in terms of its vector component beam quality factors. Then, applying the prior scalar analysis, we derived a physical expression for the M^2 factor of a general vector Schell-model source. As an example, we computed the beam quality factors for two EM Schell-model beams found in the literature using our new M^2 relation and described how to synthesize vector Schell-model beams in terms of specified, desired M^2.

To validate our analysis, we performed Monte Carlo simulations, where we generated two partially coherent sources. The simulated results were found to be in excellent agreement with the corresponding theory, and convergence to the specified, desired M^2 occurred within approximately 1000 vector field realizations. Although not performed here because of equipment availability, experimental synthesis and subsequent measurement of the M^2 factor for vector Schell-model sources can be performed using optical setups described in Refs. 15–18, 32, and 42–44.

The analysis presented in this paper will be useful in the design of vector Schell-model sources for applications from optical communications and directed energy to atomic optics and optical tweezers.

4 Appendix A: Derivation of Eq. (24)

Starting with

$$\left.\frac{\partial^2 a_{\alpha\alpha}(\boldsymbol{\rho}_d)}{\partial x_d^2}\right|_{\boldsymbol{\rho}_d=0} = \left.\frac{\partial^2}{\partial x_d^2}\left[\mathrm{jinc}\left(\frac{\rho_d}{\sqrt{2}\delta_{\alpha\alpha}}\right)\frac{1}{N}\sum_{n=1}^N \exp(-\mathrm{j}\mathbf{v}_n\cdot\boldsymbol{\rho}_d)\right]\right|_{\boldsymbol{\rho}_d=0}, \tag{44}$$

we apply the derivative multiplication rule twice to yield as follows:

$$\begin{aligned} &\left.\frac{\partial^2 a_{\alpha\alpha}(\boldsymbol{\rho}_d)}{\partial x_d^2}\right|_{\boldsymbol{\rho}_d=0} \\ &= \left.\frac{\partial}{\partial x_d}\left[\frac{1}{N}\sum_{n=1}^N \exp(-\mathrm{j}\mathbf{v}_n\cdot\boldsymbol{\rho}_d)\right]\right|_{\boldsymbol{\rho}_d=0} \left.\frac{\partial}{\partial x_d}\left[\mathrm{jinc}\left(\frac{\rho_d}{\sqrt{2}\delta_{\alpha\alpha}}\right)\right]\right|_{\boldsymbol{\rho}_d=0} \\ &+ \left.\frac{\partial}{\partial x_d}\left[\mathrm{jinc}\left(\frac{\rho_d}{\sqrt{2}\delta_{\alpha\alpha}}\right)\right]\right|_{\boldsymbol{\rho}_d=0} \left.\frac{\partial}{\partial x_d}\left[\frac{1}{N}\sum_{n=1}^N \exp(-\mathrm{j}\mathbf{v}_n\cdot\boldsymbol{\rho}_d)\right]\right|_{\boldsymbol{\rho}_d=0} \\ &+ \left.\frac{1}{N}\sum_{n=1}^N \exp(-\mathrm{j}\mathbf{v}_n\cdot\boldsymbol{\rho}_d)\right|_{\boldsymbol{\rho}_d=0} \left.\frac{\partial^2}{\partial x_d^2}\left[\mathrm{jinc}\left(\frac{\rho_d}{\sqrt{2}\delta_{\alpha\alpha}}\right)\right]\right|_{\boldsymbol{\rho}_d=0} \\ &+ \left.\mathrm{jinc}\left(\frac{\rho_d}{\sqrt{2}\delta_{\alpha\alpha}}\right)\right|_{\boldsymbol{\rho}_d=0} \left.\frac{\partial^2}{\partial x_d^2}\left[\frac{1}{N}\sum_{n=1}^N \exp(-\mathrm{j}\mathbf{v}_n\cdot\boldsymbol{\rho}_d)\right]\right|_{\boldsymbol{\rho}_d=0}. \end{aligned} \tag{45}$$

The first derivatives in Eq. (45) are odd functions of x_d; therefore, evaluating them at $\boldsymbol{\rho}_d = 0$ is trivially zero. Simplifying Eq. (45) produces as follows:

$$\begin{aligned} \left.\frac{\partial^2 a_{\alpha\alpha}(\boldsymbol{\rho}_d)}{\partial x_d^2}\right|_{\boldsymbol{\rho}_d=0} &= \left.\frac{\partial^2}{\partial x_d^2}\left[\mathrm{jinc}\left(\frac{\rho_d}{\sqrt{2}\delta_{\alpha\alpha}}\right)\right]\right|_{\boldsymbol{\rho}_d=0} \\ &+ \left.\frac{\partial^2}{\partial x_d^2}\left[\frac{1}{N}\sum_{n=1}^N \exp(-\mathrm{j}\mathbf{v}_n\cdot\boldsymbol{\rho}_d)\right]\right|_{\boldsymbol{\rho}_d=0}. \end{aligned} \tag{46}$$

We now evaluate the second derivatives in Eq. (46) separately. We begin with the second derivative of the coherence

lattice term. Bringing the derivatives inside the summation and evaluating the second derivative of the exponential yields as follows:

$$\frac{\partial^2}{\partial x_d^2}\left[\frac{1}{N}\sum_{n=1}^{N}\exp(-\mathrm{j}\mathbf{v}_n\cdot\boldsymbol{\rho}_d)\right]\Big|_{\boldsymbol{\rho}_d=0}$$
$$=\frac{1}{N}\sum_{n=1}^{N}(-\mathrm{j}v_{nx})^2\exp(-\mathrm{j}\mathbf{v}_n\cdot\boldsymbol{\rho}_d)\Big|_{\boldsymbol{\rho}_d=0}=-\frac{1}{N}\sum_{n=1}^{N}v_{nx}^2. \quad (47)$$

To evaluate the second derivative of the jinc function and argument, we first let the argument $\rho_d/(\sqrt{2}\delta_{\alpha\alpha})=u$. The associated second derivative becomes

$$\frac{\partial^2}{\partial x_d^2}\left[\mathrm{jinc}\left(\frac{\rho_d}{\sqrt{2}\delta_{\alpha\alpha}}\right)\right]=\frac{\partial}{\partial x_d}\left\{\frac{\partial u}{\partial x_d}\frac{\partial}{\partial u}\left[\frac{2J_1(u)}{u}\right]\right\}. \quad (48)$$

We now use the Bessel function identity:

$$\frac{2n}{x}J_n(x)=J_{n-1}(x)+J_{n+1}(x) \quad (49)$$

to simplify Eq. (48) to

$$\frac{\partial^2}{\partial x_d^2}\left[\mathrm{jinc}\left(\frac{\rho_d}{\sqrt{2}\delta_{\alpha\alpha}}\right)\right]=\frac{\partial}{\partial x_d}\left\{\frac{\partial u}{\partial x_d}[J_{0'}(u)+J_{2'}(u)]\right\}. \quad (50)$$

Equation (50) can be further simplified by using the Bessel function identity:

$$2J_n'(x)=J_{n-1}(x)-J_{n+1}(x), \quad (51)$$

yielding

$$\frac{\partial^2}{\partial x_d^2}\left[\mathrm{jinc}\left(\frac{\rho_d}{\sqrt{2}\delta_{\alpha\alpha}}\right)\right]=\frac{\partial}{\partial x_d}\left\{\frac{\partial u}{\partial x_d}\left[\frac{1}{2}J_{-1}(u)-\frac{1}{2}J_3(u)\right]\right\}$$
$$=-\frac{\partial}{\partial x_d}\left\{\frac{\partial u}{\partial x_d}\left[\frac{1}{2}J_1(u)+\frac{1}{2}J_3(u)\right]\right\}$$
$$=-\frac{\partial}{\partial x_d}\left\{\frac{\partial u}{\partial x_d}\frac{2J_2(u)}{u}\right\}. \quad (52)$$

In going from line 1 to 2 in Eq. (52), we used the Bessel function identity $J_{-n}(x)=(-1)^nJ_n(x)$, and in going from line 2 to 3, we used Eq. (49).

Continuing, we apply the derivative multiplication and chain rules producing

$$\frac{\partial^2}{\partial x_d^2}\left[\mathrm{jinc}\left(\frac{\rho_d}{\sqrt{2}\delta_{\alpha\alpha}}\right)\right]=-\frac{2J_2(u)}{u}\frac{\partial^2 u}{\partial x_d^2}-\left(\frac{\partial u}{\partial x_d}\right)^2\frac{\partial}{\partial u}\left[\frac{2J_2(u)}{u}\right]. \quad (53)$$

The derivative of $2J_2(u)/u$ can be found by applying Eqs. (49) and (51), such that

$$\frac{\partial^2}{\partial x_d^2}\left[\mathrm{jinc}\left(\frac{\rho_d}{\sqrt{2}\delta_{\alpha\alpha}}\right)\right]=-\frac{2J_2(u)}{u}\frac{\partial^2 u}{\partial x_d^2}-\left(\frac{\partial u}{\partial x_d}\right)^2\left[\frac{1}{4}J_0(u)-\frac{1}{4}J_4(u)\right]. \quad (54)$$

We now evaluate the first and second derivatives of u. The first derivative of u is found by applying the chain rule, namely,

$$\frac{\partial u}{\partial x_d}=\frac{1}{\sqrt{2}\delta_{\alpha\alpha}}\frac{\partial\rho_d}{\partial x_d}=\frac{1}{\sqrt{2}\delta_{\alpha\alpha}}\frac{\partial}{\partial x_d}(x_d^2+y_d^2)^{1/2}$$
$$=\frac{1}{\sqrt{2}\delta_{\alpha\alpha}}x_d\rho_d^{-1}. \quad (55)$$

The second derivative of u is found by applying the multiplication and chain rules:

$$\frac{\partial^2 u}{\partial x_d^2}=\frac{\partial}{\partial x_d}\left(\frac{1}{\sqrt{2}\delta_{\alpha\alpha}}x_d\rho_d^{-1}\right)=\frac{1}{\sqrt{2}\delta_{\alpha\alpha}}\rho_d^{-1}-\frac{1}{\sqrt{2}\delta_{\alpha\alpha}}x_d^2\rho_d^{-3}. \quad (56)$$

Substituting Eqs. (55) and (56) into Eq. (54) and simplifying produce as follows:

$$\frac{\partial^2}{\partial x_d^2}\left[\mathrm{jinc}\left(\frac{\rho_d}{\sqrt{2}\delta_{\alpha\alpha}}\right)\right]=\frac{2}{\rho_d^2}\left(1-\frac{x_d^2}{\rho_d^2}\right)J_2\left(\frac{\rho_d}{\sqrt{2}\delta_{\alpha\alpha}}\right)$$
$$-\frac{1}{8\delta_{\alpha\alpha}^2}\frac{x_d^2}{\rho_d^2}\left[J_0\left(\frac{\rho_d}{\sqrt{2}\delta_{\alpha\alpha}}\right)-J_4\left(\frac{\rho_d}{\sqrt{2}\delta_{\alpha\alpha}}\right)\right]. \quad (57)$$

Last, evaluating Eq. (57) at $\boldsymbol{\rho}_d=0$ yields as follows:

$$\frac{\partial^2}{\partial x_d^2}\left[\mathrm{jinc}\left(\frac{\rho_d}{\sqrt{2}\delta_{\alpha\alpha}}\right)\right]\Big|_{\boldsymbol{\rho}_d=0}=-\frac{1}{8\delta_{\alpha\alpha}^2}. \quad (58)$$

We obtain the second line of Eq. (24)—the desired result—by substituting Eqs. (58) and (47) into Eq. (46), i.e.:

$$\frac{\partial^2 a_{\alpha\alpha}(\boldsymbol{\rho}_d)}{\partial x_d^2}\Big|_{\boldsymbol{\rho}_d=0}=-\frac{1}{8\delta_{\alpha\alpha}^2}-\frac{1}{N}\sum_{n=1}^{N}v_{nx}^2. \quad (59)$$

Acknowledgments

The views expressed in this paper are those of the authors and do not reflect the official policy or position of the US Air Force, the Department of Defense, or the US government. The authors have no conflicts of interest.

References

1. A. E. Siegman, "New developments in laser resonators," *Proc. SPIE* **1224**, 2–14 (1990).
2. R. Martínez-Herrero and P. M. Mejías, "Second-order spatial characterization of hard-edge diffracted beams," *Opt. Lett.* **18**, 1669–1671 (1993).
3. R. Martínez-Herrero, P. M. Mejías, and M. Arias, "Parametric characterization of coherent, lowest-order Gaussian beams propagating through hard-edged apertures," *Opt. Lett.* **20**, 124–126 (1995).
4. S. Ramee and R. Simon, "Effect of holes and vortices on beam quality," *J. Opt. Soc. Am. A* **17**, 84–94 (2000).
5. F. Gori, M. Santarsiero, and A. Sona, "The change of width for a partially coherent beam on paraxial propagation," *Opt. Commun.* **82**(3), 197–203 (1991).

6. M. Santarsiero et al., "Spreading properties of beams radiated by partially coherent Schell-model sources," *J. Opt. Soc. Am. A* **16**, 106–112 (1999).
7. B. Zhang, X. Chu, and Q. Li, "Generalized beam-propagation factor of partially coherent beams propagating through hard-edged apertures," *J. Opt. Soc. Am. A* **19**, 1370–1375 (2002).
8. X. Chu, B. Zhang, and Q. Wen, "Generalized M^2 factor of a partially coherent beam propagating through a circular hard-edged aperture," *Appl. Opt.* **42**, 4280–4284 (2003).
9. S. Zhu, Y. Cai, and O. Korotkova, "Propagation factor of a stochastic electromagnetic Gaussian Schell-model beam," *Opt. Express* **18**, 12587–12598 (2010).
10. S. Zhu and Y. Cai, "M^2-factor of a stochastic electromagnetic beam in a Gaussian cavity," *Opt. Express* **18**, 27567–27581 (2010).
11. S. Zhu and Y. Cai, "M^2-factor of a truncated electromagnetic Gaussian Schell-model beam," *Appl. Phys. B* **103**, 971–984 (2011).
12. S. Zhu et al., "State of polarization and propagation factor of a stochastic electromagnetic beam in a gradient-index fiber," *J. Opt. Soc. Am. A* **30**, 2306–2313 (2013).
13. Y. Chen et al., "Vector Hermite-Gaussian correlated Schell-model beam," *Opt. Express* **24**, 15232–15250 (2016).
14. C. Liang et al., "Vector optical coherence lattices generating controllable far-field beam profiles," *Opt. Express* **25**, 9872–9885 (2017).
15. Y. Cai, Y. Chen, and F. Wang, "Generation and propagation of partially coherent beams with nonconventional correlation functions: a review," *J. Opt. Soc. Am. A* **31**, 2083–2096 (2014).
16. Y. Cai et al., "Generation of partially coherent beams," *Prog. Opt.* **62**, 157–223 (2017).
17. O. Korotkova, *Random Light Beams: Theory and Applications*, CRC, Boca Raton, Florida (2014).
18. Q. Zhan, Ed., *Vectorial Optical Fields*, World Scientific, Hackensack, New Jersey (2014).
19. H. Mao et al., "Self-steering partially coherent vector beams," *Opt. Express* **27**, 14353–14368 (2019).
20. W. Wang et al., "Recent progress on the unified theory of polarization and coherence for stochastic electromagnetic fields," *Proc. SPIE* **10612**, 10612 (2018).
21. Z. Mei, O. Korotkova, and E. Shchepakina, "Electromagnetic multi-Gaussian Schell-model beams," *J. Opt.* **15**(2), 025705 (2013).
22. S. Avramov-Zamurovic et al., "Experimental study of electromagnetic Bessel-Gaussian Schell model beams propagating in a turbulent channel," *Opt. Commun.* **359**, 207–215 (2016).
23. S. Avramov-Zamurovic et al., "Polarization-induced reduction in scintillation of optical beams propagating in simulated turbulent atmospheric channels," *Waves Random Complex Media* **24**(4), 452–462 (2014).
24. O. Korotkova, "Scintillation index of a stochastic electromagnetic beam propagating in random media," *Opt. Commun.* **281**(9), 2342–2348 (2008).
25. O. Korotkova, "Changes in the intensity fluctuations of a class of random electromagnetic beams on propagation," *J. Opt. A: Pure Appl. Opt.* **8**(1), 30–37 (2006).
26. X. Xiao and D. Voelz, "Wave optics simulation of partially coherent and partially polarized beam propagation in turbulence," *Proc. SPIE* **7464**, 74640T (2009).
27. M. W. Hyde, IV and M. F. Spencer, "Modeling the effects of high-energy-laser beam quality using scalar Schell-model sources," *Proc. SPIE* **10981**, 109810O (2019).
28. L. Mandel and E. Wolf, *Optical Coherence and Quantum Optics*, Cambridge University, New York (1995).
29. E. Wolf, *Introduction to the Theory of Coherence and Polarization of Light*, Cambridge University, New York (2007).
30. F. Gori et al., "Realizability condition for electromagnetic Schell-model sources," *J. Opt. Soc. Am. A* **25**, 1016–1021 (2008).
31. S. Basu et al., "Computational approaches for generating electromagnetic Gaussian Schell-model sources," *Opt. Express* **22**, 31691–31707 (2014).
32. M. W. Hyde et al., "Generation of vector partially coherent optical sources using phase-only spatial light modulators," *Phys. Rev. Appl.* **6**, 064030 (2016).
33. D. Voelz, X. Xiao, and O. Korotkova, "Numerical modeling of Schell-model beams with arbitrary far-field patterns," *Opt. Lett.* **40**, 352–355 (2015).
34. H. T. Yura and S. G. Hanson, "Digital simulation of an arbitrary stationary stochastic process by spectral representation," *J. Opt. Soc. Am. A* **28**, 675–685 (2011).
35. C. A. Mack, "Generating random rough edges, surfaces, and volumes," *Appl. Opt.* **52**, 1472–1480 (2013).
36. M. W. Hyde et al., "Generating partially coherent Schell-model sources using a modified phase screen approach," *Opt. Eng.* **54**(12), 120501 (2015).
37. M. W. Hyde, IV et al., "Producing any desired far-field mean irradiance pattern using a partially-coherent Schell-model source," *J. Opt.* **17**(5), 055607 (2015).
38. J. W. Goodman, *Introduction to Fourier Optics*, 3rd ed., Roberts & Company, Englewood, Colorado (2005).
39. J. D. Schmidt, *Numerical Simulation of Optical Wave Propagation with Examples in MATLAB*, SPIE Press, Bellingham, Washington (2010).
40. R. J. Sasiela, *Electromagnetic Wave Propagation in Turbulence: Evaluation and Application of Mellin Transforms*, 2nd ed., SPIE Press, Bellingham, Washington (2007).
41. I. S. Gradshteyn and I. M. Ryzhik, *Table of Integrals, Series, and Products*, 7th ed., Academic Press, Burlington, Massachusetts (2007).
42. C. Rosales-Guzmán, B. Ndagano, and A. Forbes, "A review of complex vector light fields and their applications," *J. Opt.* **20**, 123001 (2018).
43. C. Rosales-Guzmán, N. Bhebhe, and A. Forbes, "Simultaneous generation of multiple vector beams on a single SLM," *Opt. Express* **25**, 25697–25706 (2017).
44. Z. Chen et al., "Complete shaping of optical vector beams," *Opt. Express* **23**, 17701–17710 (2015).

Milo W. Hyde IV received his BS degree in computer engineering from Georgia Tech in 2001 and his MS degree and PhD in electrical engineering from AFIT in 2006 and 2010, respectively. Currently, he is an adjunct professor in the Department of Electrical and Computer Engineering at AFIT. He is a senior member of IEEE and SPIE. He is also a member of OSA and DEPS.

Mark F. Spencer is the principal investigator for the Aero Effects and Beam Control Program at the Air Force Research Laboratory, Directed Energy Directorate. He is also an adjunct assistant professor of optical sciences and engineering within the Department of Engineering Physics at the Air Force Institute of Technology. In addition to being a senior member of SPIE, he is a regular member of the Optical Society and the Directed Energy Professional Society.